Geomechanics and Engineering, *Vol. 7, No. 5 (2014) 477-493*
DOI: http://dx.doi.org/10.12989/gae.2014.7.5.477

Behaviour of micropiles in collapsible loess under tension or compression load

Zeng-zhen Qian [1a], Xian-long Lu [*2], Wen-zhi Yang [2b] and Qiang Cui [2c]

[1] *School of Engineering and Technology, China University of Geosciences, No. 29 Xueyuan Road, Haidian District, Beijing, 100083, China*
[2] *China Electric Power Research Institute, No. 15, Xiaoying East Road, Haidian District, Beijing, 100192, China*

(*Received April 05, 2014, Revised June 17, 2014, Accepted July 08, 2014*)

Abstract. This study examines the behaviour of single micropiles subjected to axial tension or compression load in collapsible loess under in-situ moisture content and saturated condition. Five tension loading tests and five compression loading tests on single micropiles were carried out at a typical loess site of the Loess Plateau in Northwest China. A series of laboratory tests, including grain size distribution, specific gravity, moisture content, Atterberg limits, density, granular components, shear strength, and collapse index, were carried out during the micropile loading tests to determine the values of soil parameters. The loess at the test site poses a severe collapse risk upon wetting. The tension or compression load-displacement curves of the micropiles in loess, under in-situ moisture content or saturated condition, can generally be simplified into three distinct regions: an initial linear, a curvilinear transition, and a final linear region, and the bearing capacity or failure load can be interpreted by the L_1-L_2 method as done in other studies. Micropiles in loess should be considered as frictional pile foundations though the tip resistances are about 10%-15% of the applied loads. Both the tension and compression capacities increase linearly with the ratio of the pile length to the shaft diameter, L/d. For micropiles in loess under in-situ moisture content, the interpreted failure loads or capacities under tension are 66%-87% of those under compression. However, the prewetting of the loess can lead to the reductions of 50% in the tensile bearing capacity and 70% in the compressive bearing capacity.

Keywords: loess; micropile; load test; ultimate load; skin friction

1. Introduction

Loess is a uniform-sized, wind-deposited soil found on most continents; however, China has some of the largest deposits on earth. The aeolian silt accumulation making up the Loess Plateau of North China approaches thicknesses of more than 250 m in the Lanzhou region (Derbyshire *et al*. 1995). Therefore, loess is a common geological formation in Northwest China.

In recent years, the construction of electricity transmission systems spannig from West to East

*Corresponding author, Ph.D., E-mail: luxianlong@163.com
[a] Ph.D., E-mail: zzqian@cugb.edu.cn
[b] M.Sc. Civil Engineer, E-mail: yangwenzhi@epri.sgcc.com.cn
[c] Ph.D., E-mail: cuiqiang@epri.sgcc.com.cn

 ISSN: 2005-307X (Print), 2092-6219 (Online)

China has been planned. Many new transmission towers must be built in this environmentally sensitive loess area. As a result, the construction of foundations for transmission towers is inevitable. Micropiles have been used in loess to support electric power transmission structures and to withstand axial and/or lateral loads. Micropiles are selected to support the electric transmission line towers to be constructed in the Loess Plateau because of their applicability to a wide range of soil conditions, the light weight of their construction equipment, and the reduction of excavation volumes.

Micropiles are small-diameter piles that can be installed in almost any type of ground where piles are required. According to the definition given in the US Federal Highway Administration (FHWA)'s micropile implementation manual (Armour *et al*. 2000), a micropile is a small-diameter drilled concrete pile (typically less than 300 mm) that is often reinforced. The micropile technique originated from experience with root piles, which were first introduced in Italy by Lizzi in the early 1950s (Lizzi 1980). Micropiles offer an alternative to conventional piling techniques and quickly spread around the world (Bruce 1989, Bruce *et al*. 1995). Micropiles have been used primarily to increase bearing capacities and reduce settlements in existing foundations (Han and Ye 2006). Some micropile studies have been carried out and published based on tests and engineering applications in several soil types (Makarchian and Poulos 1996, Jeon and Kulhawy 2001, Anil *et al*. 2004).

As an engineering material, loess is often thought of as one of the more problematic geological deposits that must be addressed by the geotechnical profession (Feda 1988). Loess deposits are susceptible to collapse when wetted; that is, collapsible loess may withstand relatively large applied vertical stresses with small settlement at low water contents, but will exhibit potentially large settlement after more extreme wetting with no additional increase in stress. The collapsibility of loess soil can be attributed to its open granular structure (Gao 1988). Engineering structures founded on the collapsible loess may be damaged by sudden and often large induced settlements when this soil is saturated after construction. Therefore, predicting the collapse potential of loess soil is important to the design of many engineering structures. Unfortunately, the tension or compression behaviours of micropiles in loess are still not well understood, and systematic full-scale tests have not yet been conducted. Thus, the design of micropiles in loess to support electric power transmission structures is typically based on empirical experience, and very limited field data are available to justify the design. The overall objectives of this study are: (i) to investigate the index properties and hydrocollapse characteristics of loess; (ii) to understand the load–displacement responses of single micropiles under compression or tension in loess under in-situ moisture content and saturated condition; and (iii) to identify the relationship of or differences between load distribution and skin friction for single micropiles under compression or tension.

2. Site conditions

A test site was selected for this study along the 750-kV Lanzhou-Tianshui-Baoji transmission line in Dingxi City, Gansu Province. This site is a typical part of the Loess Plateau in Northwest China, and was chosen for its deep, uniform deposit of loess and deep ground water.

A series of laboratory tests, including grain size distribution, specific gravity, moisture content, Atterberg limits, density, granular components, shear strength, and collapse index were carried out to determine the values of soil parameters. All the tests were performed during the micropile

loading tests to provide the most accurate soil profile when determining the soil's response to the loading. Undisturbed samples of the soil for laboratory tests were obtained by means of block sampling (300 mm × 300 mm × 150 mm blocks and 50 mm diameter cylinders). The samples were carefully trimmed and waxed from the bottom of a newly excavated 1.2-m-diameter pit from 0.7 m to 8.7 m at intervals of approximately 1.0 m in the soil profile.

Fig. 1 shows the laboratory-measured specific gravity, moisture content and density results for the in-situ soil profile. The specific gravities of these samples were found to range from 2.66 to 2.79; the average was 2.72, which is similar to the mean specific gravity values for loess that have been determined in many other parts of the world. For example, specific gravity values for the loess in Algeria are between 2.68 and 2.73 (Nouaouria *et al*. 2008), whereas those for the loess in Libya range from 2.66 to 2.73 (Assallay *et al*. 1996). As may be seen from Figs. 1(b)-(c), the moisture contents and densities are found to increase with depth and to range from 5.0% to 10.3% and from 1.28 to 1.39 g/cm^3, respectively.

The plasticity characteristics of the loess were determined by the Atterberg limits tests. Table 1 shows the typical values of Atterberg limits of loess, including liquid limit, plastic limit, and plastic index.

The particle-size distribution of the loess achieved by the combined hydrometer and sieve analysis tests according to ASTM D422 (ASTM 2007), as shown in Fig. 2. The loess can be classified as lean clay, CL, according to Unified Soil Classification System (ASTM D2487-11). Fig. 2 shows the gradation of the loess. The parameters that typically describe the shape of the particle size distribution curve, $C_u = 12.5$, $C_c = 2.88$, $D_{10} = 0.002$ mm, $D_{30} = 0.012$ mm, $D_{50} = 0.020$

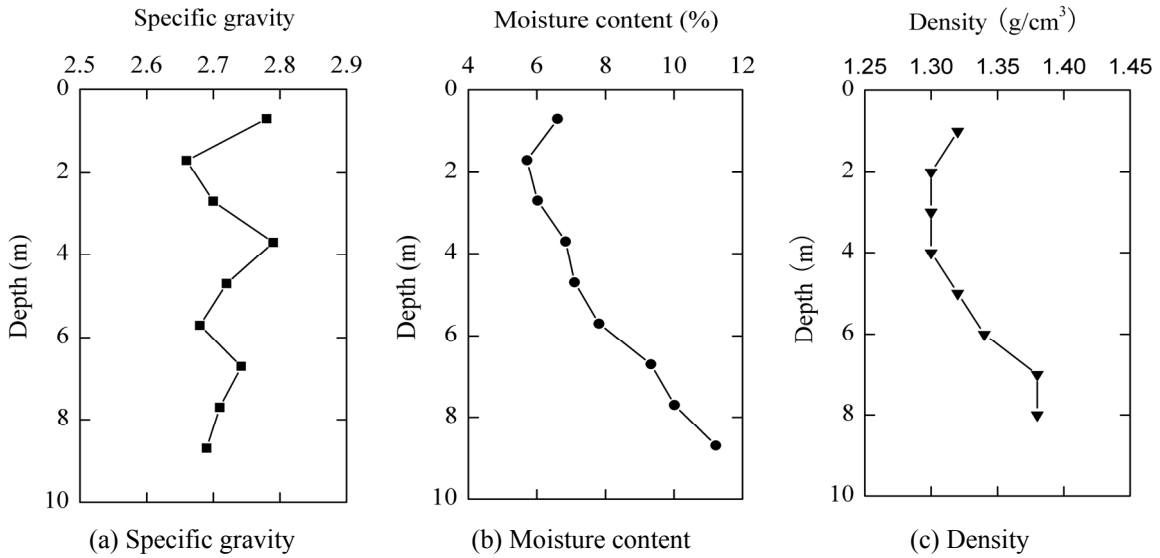

Fig. 1 Laboratory-measured results for the in-situ soil profile

Table 1 Typical value of Atterberg limits for loess

Parameter	Liquid limit, LL (%)	Plastic limit, PL (%)	Plastic index, PI
Value	31.2-34.0	16.2-20.0	11.2-17.8

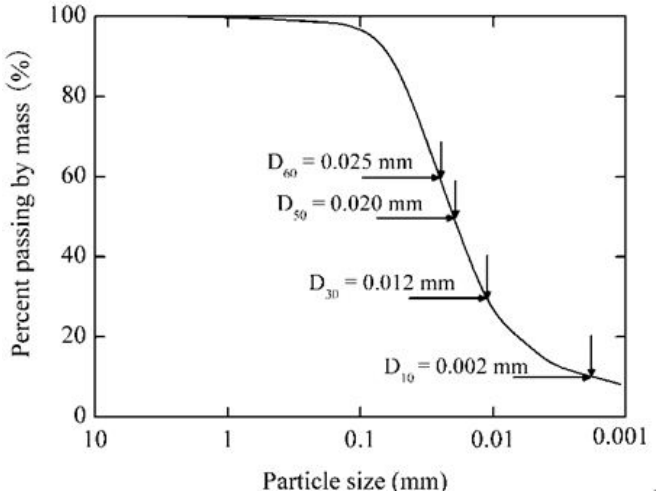

Fig. 2 Grain size distribution of the loess

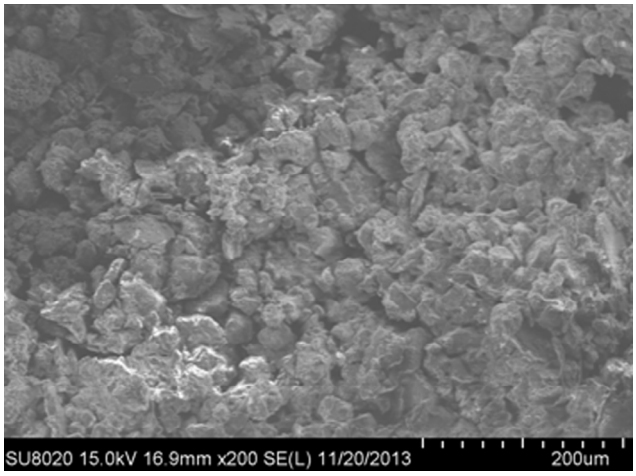

Fig. 3 Scanning electron photo-micrograph of the natural loess structure

mm, and D_{60} = 0.025 mm, indicate that the loess can be described as well-graded; that is, $C_u \geq 6$ and $1 \leq C_c \leq 3$.

The undisturbed structure and mineralogical characteristics of the loess were observed. Fig. 3 shows the scanning electron photo-micrograph of natural loess structure. This photograph shows the loose arrangement of silt particles with typical numerous voids and rootlike channels. In general, the loess unit is homogeneous and does not have internal stratification. The skeleton grains are held together mostly by means of cementation in the form of clay bridge bonds. Clay particles have smooth, sub-rounded surfaces indicating the structure of natural wind-blown deposits of loess which have not been reworked.

The X-ray diffraction analysis was run on the undisturbed soil loess to obtain the granular components. Interpretation of the X-ray data was accomplished using a computer mineral finding

program. An estimate of the amount of the dominant loess minerals was made using the peak height and peak width from X-ray diffraction patterns. The X-ray fraction analysis of the loess showed little difference in clay mineralogy between the layers. Granular components of the loess are presented in Table 2. As may be seen from Table 2, the dominant clay minerals contained in the loess are composed of illite, calcite, and kaolinite.

Direct shear tests were conducted on samples throughout the soil profile under in-situ moisture condition. Fig. 4 plots the cohesion and the friction angle of loess with depth. A crust layer was found near the ground surface; and the direct shear strength of the loess below the crust layer was found to increase with depth and to range from 16.4 to 26.9 kPa, with an average of approximately 21.5 kPa. The friction angle slightly increased with depth from 24.0 degrees in the more weathered to 29.0 degrees for the unwheathered loess, with an average of approximately 26.8 kPa.

An experimental investigation was also carried out to determine the hydrocollapsibility characteristics of the loess. There are currently two methods to evaluate and determine a soil's susceptibility to collapse, namely, the single and double oedometer tests. According to the previous studies (Lawton *et al*. 1989, Basma and Tuncer 1992, Lim and Miller 2004), these two techniques yield similar results. The single oedometer test was selected because the wetted-after-loading approach more closely resembles the conditions of compacted soils in the field. Consequently, the experimental data on the hydrocollapsibility characteristics of loess discussed in this study were based on the results obtained from the single oedometer test. A total of nine groups, each consisting of three undisturbed soil specimens (79.8 mm in diameter and 20 mm in height), were performed. Each test consisted of placing a soil specimen at the in-situ moisture content in a consolidometer, applying a predetermined vertical pressure of 200 kPa to the specimen and

Table 2 Clay species composing the total clay fraction of the loess at test site

Mineral	Illite	Calcite	Kaolinite	Montmorillonite	Chlorite	Vermiculite	Iron oxides	Others
Fraction (%)	47	19	13	6	6	5	3	1

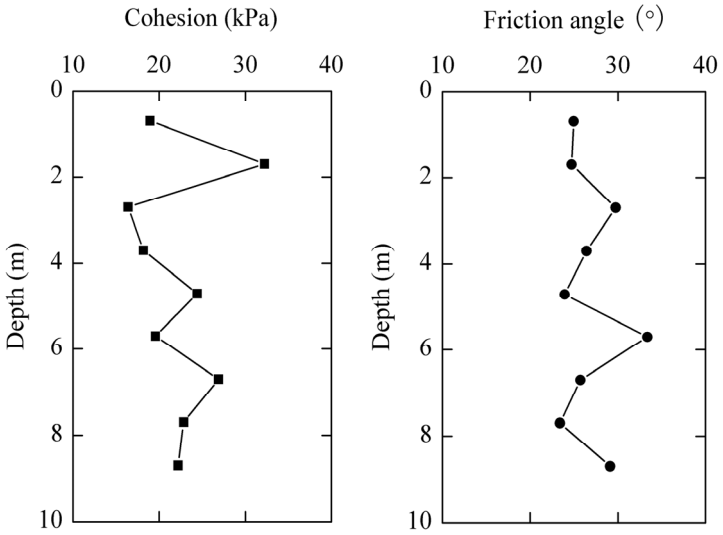

Fig. 4 Direct shear test results of cohesion and friction angle for the loess profile

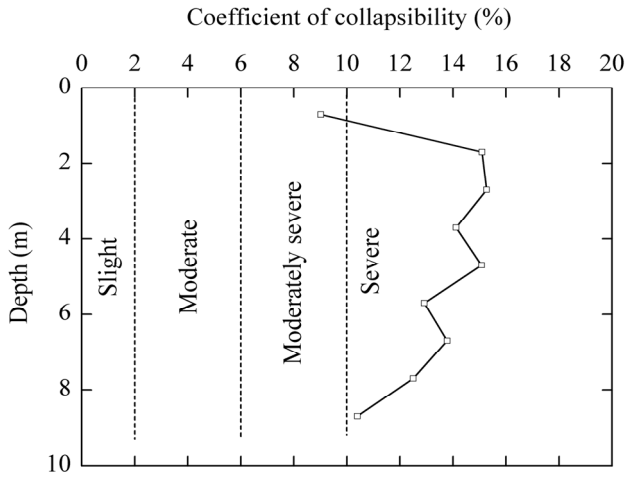

Fig. 5 Classification of the collapse index and corresponding test results for the soil profile

inundating the specimen with water to induce the collapse of the soil specimen. The test procedure essentially followed the criteria recommended in ASTM D5333 (ASTM 2003). The curve shown in Fig. 5 illustrates the classification of the collapse index and corresponding average test values of the collapse index for the soil profile, as well as the magnitude of the decrease in the hydrocollapse with increasing depth. For a stress of 200 kPa, the average measured magnitudes of hydrocollapse of the specimens vary from 9.0% to 15.3%. Based on the classification values of the collapse index suggested by ASTM D5333 (ASTM 2003), the loess in this test site can be concluded to pose a severe collapse risk.

Based on a comparison of Figs. 1(b)-(c) and Fig. 5, it is clear that the collapse potential generally decreases with increasing initial density and moisture content. This conclusion is consistent with the reports by Basma and Tuncer (1992) and Lim and Miller (2004). Physically, this trend implies that denser soils have lower initial void ratios and are at lower risk of collapse upon wetting. Similarly, a soil that is wetter at compaction has a lower collapse index. The collapse potential is reduced because the initial bond provided by the fine fractions in the soil is weakened by the higher initial amount of water.

3. Test foundation and installation

Ten micropiles were installed at the test site. Three of these micropiles, numbered from $MP1^T$ to $MP3^T$, were tested under tension in loess under in-situ moisture content. Two micropiles, numbered $MP4^T$ and $MP5^T$, were tested under tension in loess under saturated condition. Three micropiles, numbered from $MP1^C$ to $MP3^C$, were tested under compression in loess under in-situ moisture content. Two micropiles, numbered $MP4^C$ and $MP5^C$, were tested under compression in loess under saturated condition.

All of the micropiles were drilled without groundwater being encountered. After the drill reached the desired depth, a nominal 200 mm diameter steel-reinforced cage with eight 16 mm steel rebars 45° apart around the centerline was inserted into the predrilled hole. After the cage

was placed, a sleeved grout pipe was put in the center of the hole. Sulphate-resistant concrete formed by aggregates finer than 25 mm with cement, with a 28-day compressive strength of 30 MPa, was poured by free fall to the top of the pile. The quality of the installed shafts was guaranteed by manually vibrating during concrete pouring. After hardening of the initially placed concrete, approximately 3 to 4 hours, grouting was carried out for all micropiles. Grouting pressure varied between 0.8 and 1.0 MPa with a high pressure of 1.5 MPa at the beginning. The cement/water ratio used in this study was 0.5. Low strain integrity tests were done for assessing the quality of shaft construction prior to compression or tension loading. According to the low strain integrity testing results, there was no defect on connection for all the micropiles.

For all of the micropiles installed for this study, the nominal shaft diameter, d, was equal to 0.30 m, and the nominal pile length, L, ranged from 6 to 10 m, as presented in Table 3. The ratios of the pile length to the shaft diameter, L/d, ranged from 20 to 33.3.

According to the micropile classification method (based on type of grouting) recommended in the FHWA implementation manual (Armour *et al*. 2000), the micropiles discussed in this study may be classified as type B. However, the micropiles in China to support electric power transmission line structures have two distinct differences from the typical micropiles in the United States. Firstly, the micropiles in the United States use a single, large-diameter (25-63 mm) rebar, instead of a steel-reinforced cage. Secondly, neat cement grouts are commonly used in the United States, instead of the sulphate-resistant concrete formed by aggregates with cement used in study. Because of the relatively low compressive strength of the grout used for the micropiles in the United States, the large rebar carries and transfers most of the applied load.

4. Loess prewetting

Loess for four micropile tests (i.e., $MP4^T$, $MP5^T$, $MP4^C$, and $MP5^C$) were thoroughly prewetted by ponding prior to the tension or compression tests. Fig. 6 presents the prewetting arrangement of loess by ponding for a micropile. Water was poured into a round pit approximately 600 mm in depth, and 1500 mm and 1200 mm in top and bottom diameter, respectively. As may be seen from Fig. 6, this special technique of water adding can ensure a gradual and uniform infiltration of water around the micropile. Four predrilled holes with diameters of 100 mm were symmetrically arranged along a 1000-mm-diameter circle 90° apart around the centerline, and were approximately 500 mm deeper than the tested micropile. A 20-mm-diameter polyvinyl chloride (PVC) tube was placed at the center of each predrilled hole. Two 5-mm-diameter holes were symmetrically arranged at the same cross section using 200-mm spacing, along each PVC tube. Fine sand was used to fill the gap between the hole and the PVC tube.

Fig. 7 is the photographs of water supplying and prewetting arrangements in progress for a tension and a compression micropile, respectively. During the prewetting, the water level in the pit was maintained at approximately 0.15 m above the portholes of the PVC tubes. As Fig. 7 shows, the round pit was covered with the plastic cloth to ensure that the loess around the test pile would be fully wetted in the vertical direction. This method of soil prewetting eliminated the problem of the sudden and erratic loess collapse.

Fig. 8 shows the relationships between the total poured water volume and the prewetting time. As can be seen from Fig. 8, about forty-five cubic meters of water were generally poured into the loess and allowed to seep downward into the soil. The curves shows a gradual rise from the beginning to the prewetting time of 95 h, and the curve of total water volume, Q, and prewetting

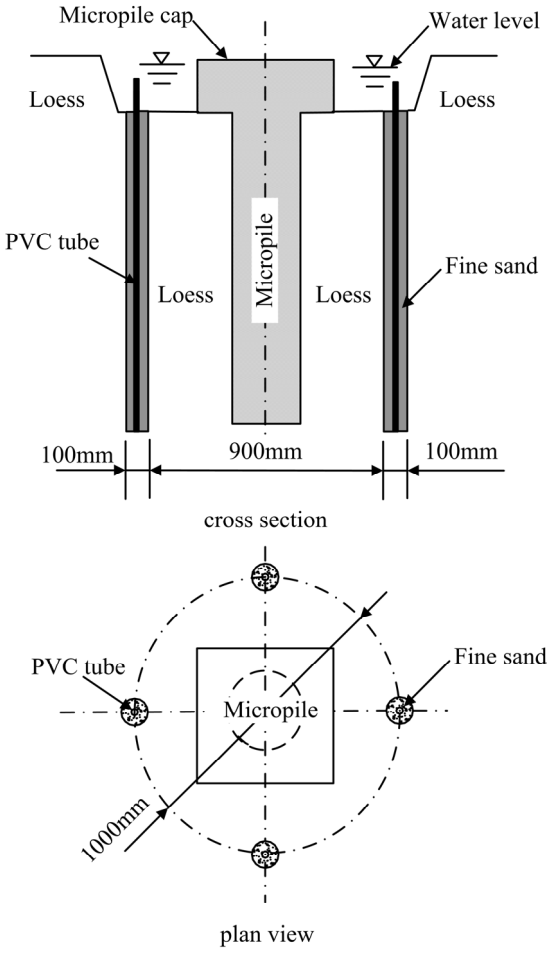

Fig. 6 Prewetting arrangement of loess by ponding

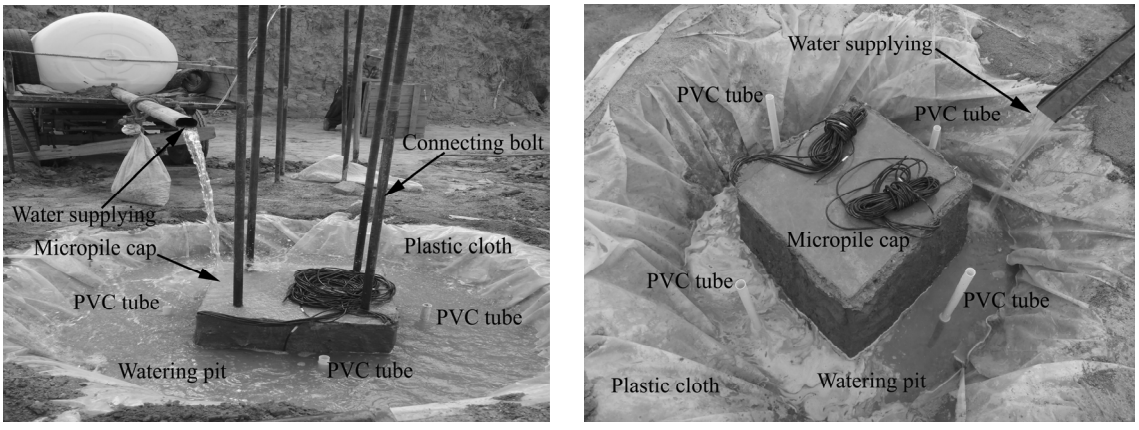

(a) Tension-loaded micropile (b) Compression-loaded micropile

Fig. 7 Loess prewetting in progress

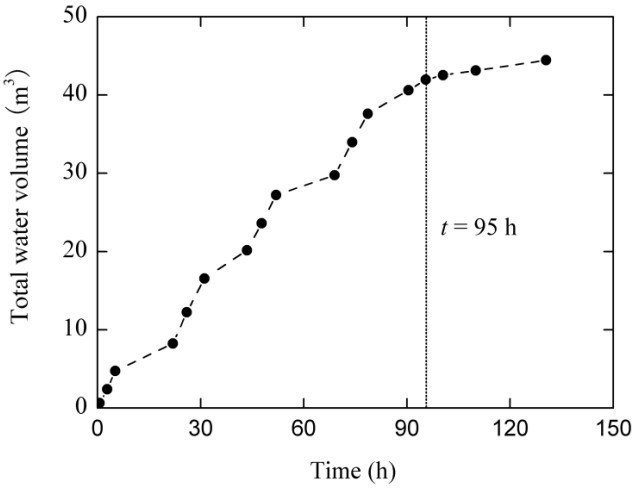

Fig. 8 Relationship between the total poured water volume and the prewetting time

time, t, could be fitted by $Q = 0.465t$, namely 0.465 m^3/h. However, after a sufficient prewetting period about 95 hours, the curve follows by a very low increment ratio of poured watering. Gibbs and Holland (1960) concluded that maximum dry strength occurs at moisture contents below 10 percent and high resistance to settlement should be expected. Soils with moisture contents between 10 to 15 percent have moderately high strength, with strength declining as moisture approaches 20 percent. Moisture contents above 20 percent are considered high and will permit full consolidation to occur under load. Saturation occurs at about 35 percent moisture. Therefore, the prewetted loess discussed in this study during the compression or tension load tests could be considered as under saturated condition.

5. Loading procedure and test method

Each load test was conducted after the concrete had cured for approximately 28 days. The test setup and test method were designed according to the criteria recommended in CEI/IEC 1773 (CEI/IEC 1996). The same loading, reaction, instrumentation, and data acquisition systems were used for all single micropile tests.

Fig. 9 is the photographs of the tension and compression test setups in progress. As observed, the axial load was applied with a hydraulic jack aligned with the central longitudinal axis of the micropile. The corresponding axial displacement was measured by two electronic gauges with a range of 50 mm and a sensitivity of 0.01 mm. The gauges were attached to a reference beam installed over the test micropile. The reference beam was of sufficient stiffness to support the instrumentation so that excessive variations in readings did not occur.

All of the tests were conducted with static loading without load cycling. The slowly maintained load method was adopted in all tests; that is, the tension or compression loading was applied in increments of 10% of the predicted ultimate load of each micropile, and the micropile was allowed to axially move under each maintained-load increment until a certain rate of displacement was achieved. Each load increment was maintained after loading until two consecutive displacements

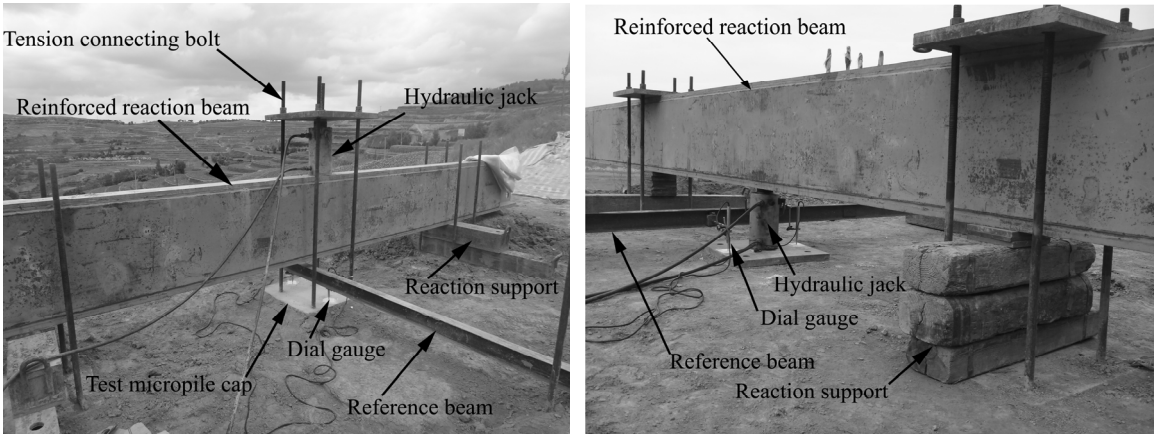

(a) Load test of micropile undere tension (b) Load test of micropile undere compression

Fig. 9 Experimental setup for tension and compression loading system in progress

within each hour were less than 0.1 mm. Then, the next increment of load was added. A tension or compression test was continued up to the point of failure, or the test was terminated after the last load was maintained for 24 hours with the rate of displacement exceeding the above criteria. Consequently, the load-carrying capacity of the micropile was considered the peak load, and the test was halted when the peak load was achieved. Therefore, there was no drop in tension or compression resistance after the peak was reached in the load-displacement curve. In general, the micropile load tests discussed in this study were conducted in accordance with ASTM D3689-90 (ASTM 1995). This is also the typical test procedure recommended by the Chinese National Code GB50007 (CNC 2011) and Local Code JGJ 94 (CLC 2008).

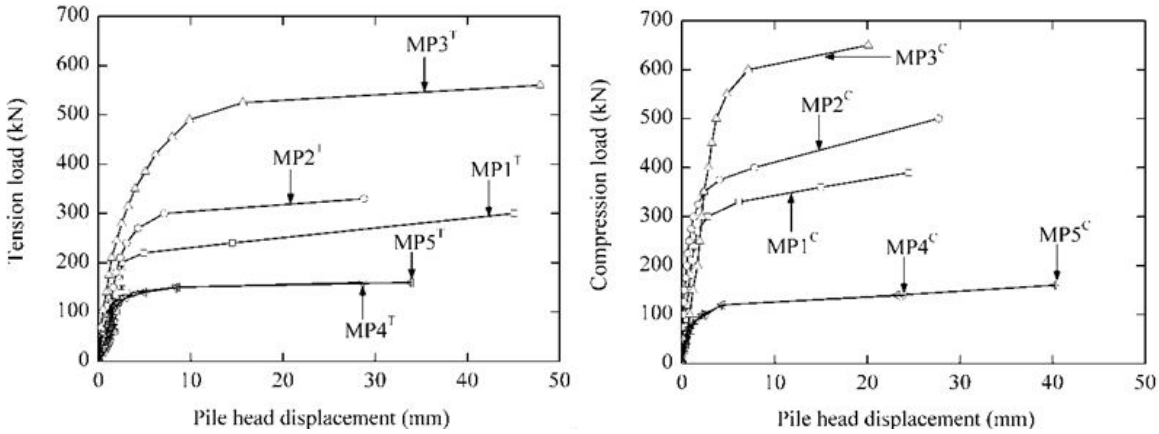

(a) Micropiles under tension (b) Micropiles under compression

Fig. 10 Measured load-displacement curves in the field tests

6. Analysis of test results

6.1 Load-displacement responses

Load tests often are used to validate a foundation design, and they provide a basis for evaluating the prediction of load-carrying capacity. Therefore, it is essential to understand the load-displacement behaviour of a given foundation system and to interpret the load test results. The results of the load tests of micropile under compression or tension presented herein are discussed in terms of load-displacement behaviour. Fig. 10 presents the load-displacement responses of all micropiles. The load–displacement responses in Fig. 10 clearly indicate that the micropiles in loess loaded under in-situ moisture content had higher load capacities than those loaded under saturated condition.

6.2 Interpreted loads and displacements

As may be seen from Fig. 10, the axial load-displacement responses almost follow the same pattern, which are similar to those of drilled shafts under axial uplift loading in gravelly and non-gravelly soils (Chen *et al*. 2008, Chen and Chu 2012), and to those of drilled shafts under axial uplift loading in Gobi gravel (Qian *et al*. 2014). These axial load-displacement curves can generally be simplified into three distinct regions, i.e., an initial linear region, a curvilinear transition region, and a final linear region, as illustrated in Fig. 11. Beyond the end of the transition region, within the final linear region, a small increase in load produces a significant increase in settlement. The final portion of the curve is not typically asymptotic to any finite value; thus, the bearing capacity or failure load must be interpreted from load test results as done in previous studies (Akbas and Kulhawy 2009, Briaud 2007, Chen and Chu 2012, Chen and Fang 2009, Chen *et al*. 2008, Qian *et al*. 2014).

The L_1-L_2 method proposed by Hirany and Kulhawy (1988, 1989, 2002) is useful for interpreting the type of load-displacement curve obtained in this study. As Fig. 11 shows, point L_1 (the elastic limit) corresponds to the load (T_{L1}) and displacement (s_{L1}) at the end of the initial linear

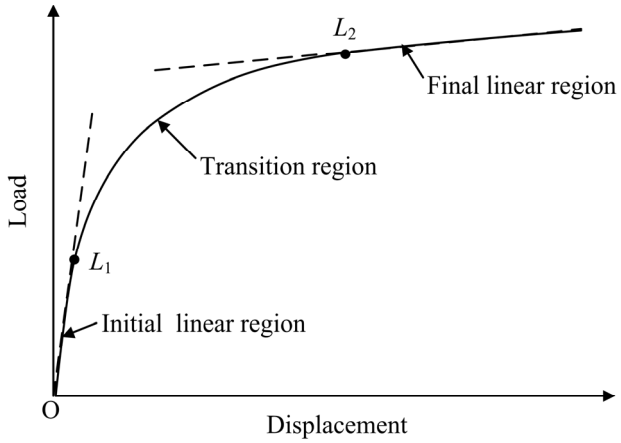

Fig. 11 Regions of the load-displacement curve and the definition of L_1-L_2 method for capacity interpretation criterion

region, whereas L_2 (the failure threshold) corresponds to the load (T_{L2}) and displacement (s_{L2}) at the beginning of the final linear region. T_{L2} is defined as the interpreted failure load or capacity because beyond T_{L2}, a small increase in load leads to a significant increase in displacement. This criterion for evaluating the load capacities is also consistent with the findings of Jeon and Kulhawy (2001). The values of the interpreted loads T_{L1} and T_{L2}, as well as the corresponding displacements s_{L1} and s_{L2}, are provided in Table 3.

The micropiles could be considered as frictional pile foundations due to the large ratios of length to shaft diameter, L/d. The vertical tensile and compressive load-carrying capacities were mainly determined from the shaft friction and pile length. The results in Table 3 indicate that both the compressive and the tensile load-bearing capacity increase linearly with increasing L/d, as shown in Fig. 12. However, Table 3 indicates that the ratios of T_{L1}/T_{L2} for tension-loaded single micropiles in loess under in-situ moisture content range from 0.90 to 0.40 and decrease with

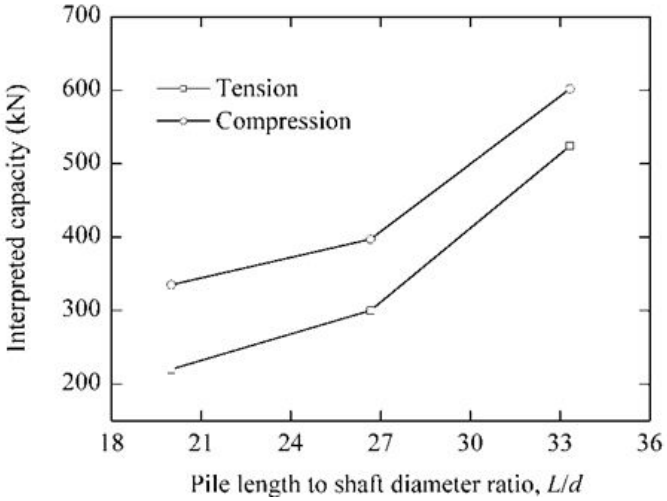

Fig. 12 Interpreted load capacities versus pile length to shaft diameter, L/d

Table 3 Basic information on tests and interpreted load-displacement results

Axial loading type	Pile number	Moisture condition	L (m)	D (m)	T_{L1} (kN)	s_{L1} (mm)	T_{L2} (kN)	s_{L2} (mm)	T_{L1}/T_{L2}
Uplift	MP1^{T}	In-situ	6.0	0.3	198	2.31	220	4.91	0.90
	MP2^{T}	In-situ	8.0	0.3	211	2.33	300	7.12	0.70
	MP3^{T}	In-situ	10.0	0.3	212	1.32	525	15.66	0.40
	MP4^{T}	Saturated	8.0	0.3	109	1.59	150	8.43	0.73
	MP5^{T}	Saturated	8.0	0.3	121	1.67	150	8.55	0.81
Compression	MP1^{C}	In-situ	6.0	0.3	231	1.14	335	6.85	0.69
	MP2^{C}	In-situ	8.0	0.3	274	0.92	397	7.46	0.69
	MP3^{C}	In-situ	10.0	0.3	456	3.24	602	7.16	0.76
	MP4^{C}	Saturated	8.0	0.3	84	1.35	120	4.61	0.70
	MP5^{C}	Saturated	8.0	0.3	73	0.75	119	4.35	0.61

increasing L/d. For compression-loaded micropiles, the ratios of T_{L1}/T_{L2} are found to range from 0.69 to 0.76 with a mean ratio of 0.71 and increase with increasing L/d.

The results in Table 3 and Fig. 12 indicate that the interpreted failure loads or capacities under tension in loess under in-situ moisture content are approximately 66%-87% of those under compression. The lower load capacities of the micropiles under tension may result from the stress field around the pile and in the soil being different when the micropiles are subjected to compression from when they are subjected to tension. Micropiles tend to expand under compressive loads and contract under tensile loads. Because of Poisson's ratio effect, the normal stress at the pile-soil interface increases under compression but decreases under tension. This variation in the normal stress may be a significant factor influencing the magnitude of the ratio of the tensile to the compressive shaft capacity of a micropile.

However, the tension and compression capacities of a single micropile in loess under saturated condition are approximately 50% and 30%, respectively, of those in loess under in-situ moisture content; that is, the prewetting of loess leads to reductions of 50% in tension bearing capacity and 70% in compression bearing capacity.

6.3 Axial forces in micropiles

In order to investigate the mechanism of load transfer, strain sensors were attached to the reinforcing bars of each micropile at the depth of 2.0 m, 4.0 m, 6.0 m, and 7.5m.

It is assumed that the reinforcing bar can be fully bonded with concrete. Therefore, the strain in the reinforcing bar is equal to that in concrete. Based on the measured stain at a certain depth, z, the average axial force at that depth in each micropile can be calculated as follows

$$F_z = E_p A_p \varepsilon_z \tag{1}$$

where F_z is the axial force back-calculated from the measured strain at a certain depth z; A_p is the area of the micropile cross section; ε_z is the average axial strain of reinforcing bar at a certain depth z; E_p = the the Young's modulus of pile concrete (according the compressive test, E_c = 31.5 GPa).

The distributions of four typical axial forces in the micropiles with depth, under compression or tension, are presented in Fig. 13. The distributions show that the axial forces increase with the applied loads on the micropile heads but decrease with depth because of skin friction. Tip resistance existed in the micropiles under compression ($MP2^C$ and $MP5^C$), but almost not in the micropiles under tension ($MP2^T$ and $MP5^T$). Tip resistance was about 10-15% of the applied load. These findings are consistent with those reported by Han and Ye (2006) and Qian and Lu (2011).

6.4 Average skin friction along the micropiles

The average skin friction for each pile was determined by dividing the load applied to the pile head by the total surface area of the micropile. Fig. 14 presents the variation in average skin friction with pile head displacements for the 10 micropiles. As may be seen from Fig. 14, the average skin friction along the length of the micropiles generally increases with the increasing of the applied loads and corresponding pile head displacements. However, in loess under in-situ moisture content, the average skin friction for micropiles under the interpreted failure compression load is approximately 25% higher than that under tension; i.e., the average skin friction is about

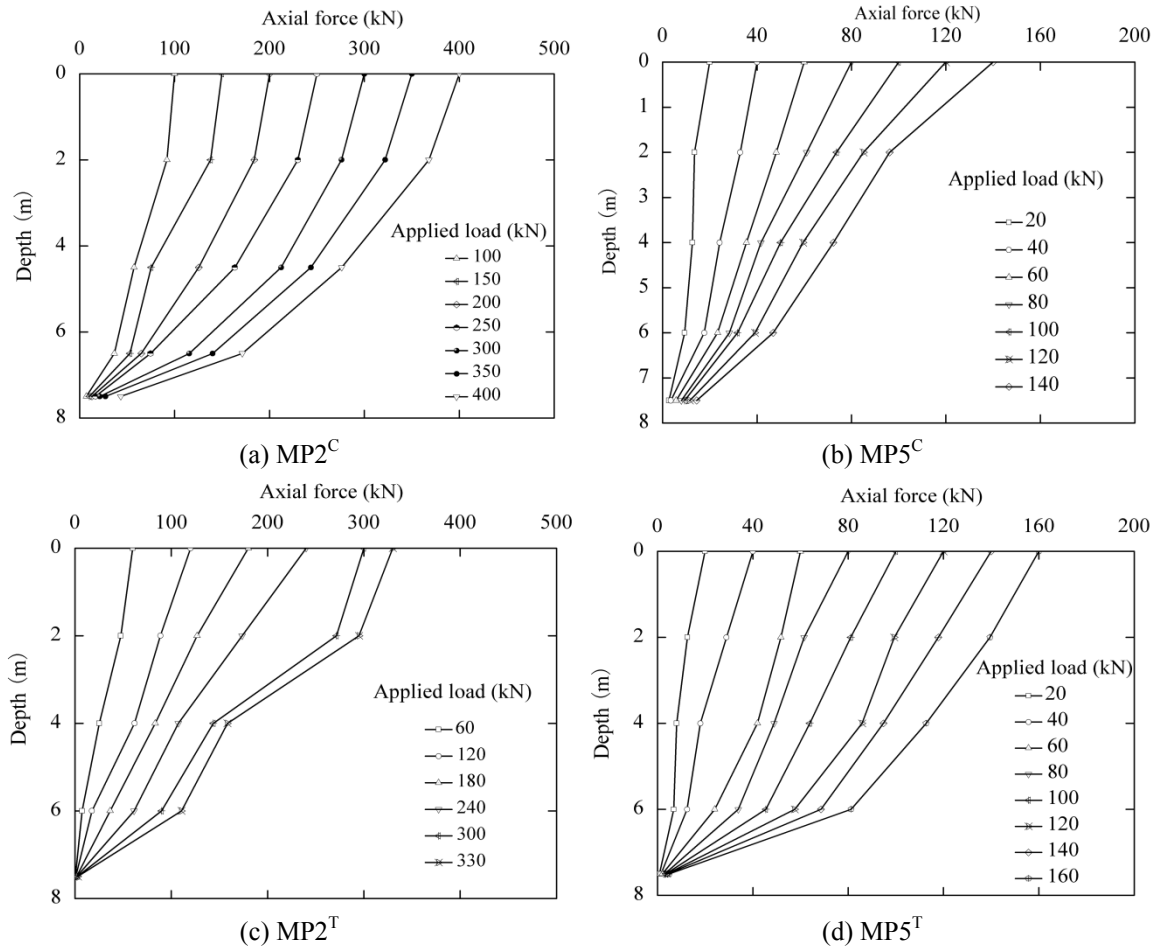

Fig. 13 Axial load distribution in micropile

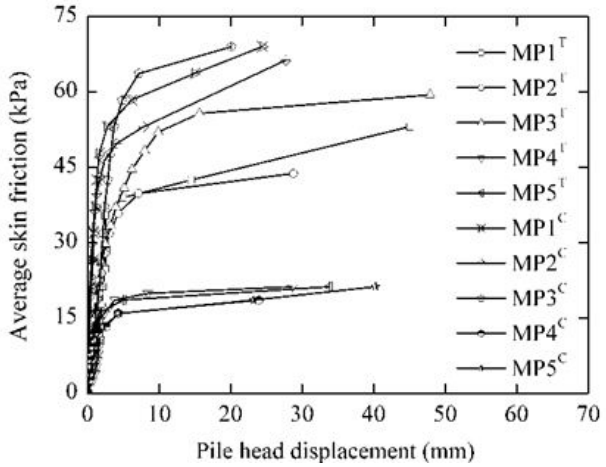

Fig. 14 Average skin friction versus pile head displacement

44.8 kPa under the interpreted failure tensile load and 60.2 kPa under the corresponding compressive load. However, in the saturated loess, these values are 19.2 and 15.9 kPa for the interpreted failure tensile and compressive loads, respectively.

7. Conclusions

The following conclusions can be drawn based on the results of the field load tests on the behaviour of single micropiles subjected to tension or compression load in loess under in-situ moisture content and saturated condition, respectively:

(1) The loess at the test site is a typical part of the Loess Plateau in Northwest China, and poses a severe collapse risk upon wetting.
(2) The axial load-displacement curves of the micropiles in loess, under in-situ moisture content or saturated condition, are nonlinear and can be divided into three distinct regions: initial linear, curvilinear transition, and final linear region, and the bearing capacity or failure load can be interpreted by the L_1-L_2 method as done in other studies.
(3) A micropile in loess should be considered as frictional pile foundation though the tip resistance is about 10-15% of the applied load, and the compression or tension load-carrying capacities of micropiles in loess increase linearly with the increasing ratio of the pile length to the shaft diameter, L/d.
(4) For micropiles in loess under in-situ moisture content, the interpreted failure loads or capacities under tension are 66%-87% of those under compression. However, prewetting of the loess leads to reductions of 50% in the tensile bearing capacity and 70% in the compressive bearing capacity, respectively.
(5) The average skin friction along the micropiles increased with the increasing of the applied loads and pile head displacements. In loess under in-situ moisture content, the average skin friction under compression at failure is approximately 25% higher than that under tension, with the values of 60.2 kPa and 44.8 kPa, respectively. However, in saturated loess, the skin friction values at failure are 19.2 kPa and 15.9 kPa for tension and compression loading, respectively.

Acknowledgments

The authors wish to acknowledge the support provided by the National Natural Science Foundation of China (No. 51208480) and the Fundamental Research Funds for Central Universities (No. 53200959614).

References

Akbas, S.O. and Kulhawy, F.H. (2009), "Axial compression of footings in cohesionless soils. I: Load-settlement behavior", *J. Geotech. Geoenviron. Eng.*, **135**(11), 1562-1574.

Anil, M., Chen, C.H. and Oberoi, R. and Kleiber, A. (2004), "Simplified analysis method for micropile pullout behavior", *J. Geotech. Geoenviron. Eng.*, **130**(10), 1024-1033.

Armour, T., Groneck, P., Keeley, J. and Sharma, S. (2000), "Micropile design and construction guidelines implementation manual priority technologies program (PTP) project", Rep. No. FHWA-SA-97-070,

Department of Transportation Federal Highway, Washington, D.C., USA, pp. 32-33.
Assallay, A.M., Rogers, C.D.F. and Smalley, I.J. (1996), "Engineering properties of loess in Libya", *J. Arid Environ*., **32**(4), 373-386.
ASTM (1995), Standard test method for individual piles under static axial tensile load, ASTM D3689-90(1995), American Society for Testing and Materials; ASTM International, West Conshohocken, PA, USA.
ASTM (2003), Standard test method for measurement of collapse potential of soils, ASTM D5333 – 2003, American Society for Testing and Materials; ASTM International, West Conshohocken, PA, USA.
ASTM (2007), Standard test method for particle-size analysis of soils, ASTM D422-63, American Society for Testing and Materials; ASTM International, West Conshohocken, PA, USA.
ASTM (2011), Standard practice for classification of soils for engineering purposes (Unified Soil Classification System), ASTM D2487-11, American Society for Testing and Materials; ASTM International, West Conshohocken, PA, USA.
Basma, A.A. and Tuncer, E.R. (1992), "Evaluation and control of collapsible soils", *J. Geotech. Eng. Div*., **118**(10), 1491-1504.
Briaud, J.L. (2007), "Spread footings in sand: Load settlement curve approach", *J. Geotech. Geoenviron. Eng*., **133**(8), 905-920.
Bruce, D.A. (1989), "Aspects of minipiling practice in the United States", *Ground Eng*., **22**(1), 35-39.
Bruce, D.A., Dimillio, A.F. and Juran, I. (1995), "Introduction to micropiles: An international perspective", *Foundation Upgrading and Repair for Infrastructure Improvement*, (William F.K. and John M.T. Eds.), ASCE, New York, GSP(50), pp. 1-26.
CEI/IEC (1996), Overhead lines-Testing of foundation for structures, CEI/IEC 1773, Commission Electrotechinque Internationale / International Electrotechnical Commission, Bureau central de la Commission Electrotechnique Internationale 3, Geneva, Switzerland.
Chen, Y.J. and Chu, T.H. (2012), "Evaluation of uplift interpretation criteria for drilled shafts in gravely soils", *Can. Geotech. J*., **49**(1), 70-77.
Chen, Y.J. and Fang, Y.C. (2009), "Critical evaluation of compression interpretation criteria for drilled shafts", *J. Geotech. Geoenviron. Eng*., **135**(8), 1056-1069.
Chen, Y.J., Chang, H.W. and Kulhawy, F.H. (2008), "Evaluation of uplift interpretation criteria for drilled shaft capacity", *J. Geotech. Geoenviron. Eng*., **134**(10), 1459-1468.
CLC (2008), Technical code for building pile foundations, Chinese Local Code JGJ 94-2008, China Architecture and Building Press, Beijing, China. [In Chinese]
CNC (2011), Code for design of building foundations, Chinese National Code GB50007-2011, China Architecture and Building Press, Beijing, China. [In Chinese]
Derbyshire, E., Meng, X.M. and Wang, J.T., Zhou, Z.Q. and Li, B.X. (1995), "Collapse loess on the loess plateau of China", *Genesis*, *properties of Collapsible Soils*, (Derbyshire E., Dijkstra T. and Smalley I.J. Eds.), Kluwer, Dordrecht, The Netherlands, pp. 267-293.
Feda, J. (1988), "Collapse of loess upon wetting", *Eng. Geol*., **25**(2-4), 263-269.
Gao, G.R. (1988), "Formation and development of the structure of collapsing loess in china", *Eng. Geol*., **25**(2-4), 235-245.
Gibbs, H.J. and Holland, W.Y. (1960), "Petrographic and engineering properties of loess", Engineer Monograph No. 28, U.S. Bureau of Reclamation, Denver, CO, USA, 37 p.
Han, J. and Ye, S.L. (2006), "A field study on behavior of micropiles under compression or tension", *Can. Geotech. J*., **43**(1), 19-29.
Hirany, A. and Kulhawy, F.H. (1988), "Conduct and interpretation of load tests on drilled shaft foundations: Detailed guidelines", Report No. EPRI EL-5915, Electric Power Research Institute, Palo Alto, CA, USA, pp. 272-273.
Hirany, A. and Kulhawy, F.H. (1989), "Interpretation of load tests on drilled shafts. II: Axial uplift", *Foundation Engineering*: *Current Principles and Practices*, (Kulhawy FH Eds.), ASCE, New York, (GSP 22), pp. 1150-1159.
Hirany, A. and Kulhawy, F.H. (2002), "On the interpretation of drilled foundation load test results", *Deep*

foundations, (O'Neill M.W. and Townsend F.C. Eds.), ASCE, Reston, VA, (GSP 22), pp. 1018-1028.
Jeon, S.S. and Kulhawy, F.H. (2001), "Evaluation of axial compression behavior of micropiles", *Proceedings of Foundation and Ground Improvement*, (Brandon T.L. Eds.), ASCE, Reston, VA, (GSP 113), pp. 460-471.
Lawton, E.C., Fragaszy, R.J. and Hardcastle, J.H. (1989), "Collapse of compacted clayey sand", *J. Geotech. Geoenviron. Eng.*, **115**(9), 1252-1267.
Lim, Y.Y. and Miller, G.A. (2004), "Wetting-induced compression of compacted Oklahoma soils", *J. Geotech. Geoenviron. Eng.*, **130**(10), 1014-1023.
Lizzi, F. (1980), *The Use of Root Pattern Piles in the Underpinning of Monuments and Old Buildings and in the Consolidation of Historic Centres*, L'Industria delle Costruzioni, Volume 110, p. 25.
Makarchian, M. and Poulos, H.G. (1996), "Simplified method for design of underpinning piles", *J. Geotech. Geoenviron. Eng.*, **122**(9), 745-751.
Nouaouria, M.S., Guenfoud, M. and Lafifi, B. (2008), "Engineering properties of loess in Algeria", *Eng. Geol.*, **99**(1-2), 85-90.
Qian, Z.Z and Lu, X.L. (2011), "Behavior of micropiles in soft soil under vertical loading", *Adv. Mater. Res.*, **243-249**, 2143-2150.
Qian, Z.Z., Lu, X.L. and Yang, W.Z. (2014), "Axial uplift behavior of drilled shafts in Gobi gravel", *Geotech. Test. J.*, **37**(2), 205-217.

CC